LightGaussian: Unbounded 3D Gaussian Compression with 15x Reduction and 200+ FPS

Zhiwen Fan[1*], Kevin Wang[1*], Kairun Wen[2], Zehao Zhu[1], Dejia Xu[1], Zhangyang Wang[1]
[1]University of Texas at Austin, [2]Xiamen University

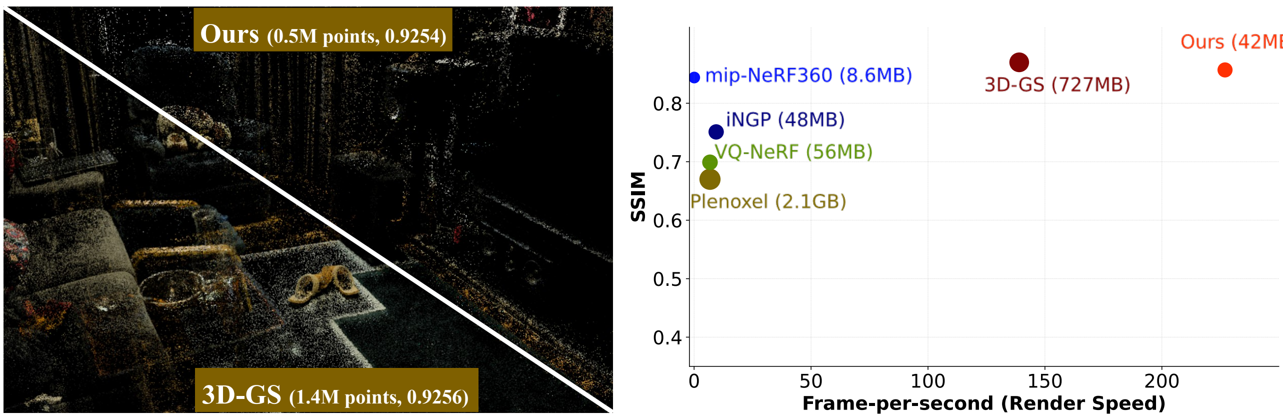

Figure 1. **Compressibility and Rendering Speed**. We present **LightGaussian** to transform 3D Gaussians into a more compact representation. LightGaussian effectively prunes redundant Gaussians while preserving visual fidelity (on the left). Consequently, it reduces the average storage from 727MB to 42MB and improves the FPS from 139 to 215.

Abstract

*Recent advancements in real-time neural rendering using point-based techniques have paved the way for the widespread adoption of 3D representations. However, foundational approaches like 3D Gaussian Splatting come with a substantial storage overhead caused by growing the SfM points to millions, often demanding gigabyte-level disk space for a single unbounded scene, posing significant scalability challenges and hindering the splatting efficiency. To address this challenge, we introduce **LightGaussian**, a novel method designed to transform 3D Gaussians into a more efficient and compact format. Drawing inspiration from the concept of Network Pruning, LightGaussian identifies Gaussians that are insignificant in contributing to the scene reconstruction and adopts a pruning and recovery process, effectively reducing redundancy in Gaussian counts while preserving visual effects. Additionally, LightGaussian employs distillation and pseudo-view augmentation to distill spherical harmonics to a lower degree, allowing knowledge transfer to more compact representations while maintaining scene appearance. Furthermore, we propose a hybrid scheme, VecTree Quantization, to quantize all attributes, resulting in lower bitwidth representations with minimal accuracy losses. In summary, LightGaussian achieves an averaged compression rate over 15× while boosting the FPS from 139 to 215, enabling an efficient representation of complex scenes on Mip-NeRF 360, Tank & Temple datasets. Project website:* `https://lightgaussian.github.io/`

1. Introduction

Novel view synthesis (NVS) aims to generate photo-realistic images of a 3D scene from unobserved viewpoints, given a set of calibrated multi-view images. NVS holds importance as it can be used for a wide range of real-world applications, including virtual reality [11], augmented reality [68], digital twin [12], and autonomous driving [60]. Neural Radiance Fields (NeRFs)[4, 5, 40] have demonstrated promising ability for photo-realistic 3D modeling and synthesis from multi-view images where 3D location and view directions are mapped to view-dependent color and volumetric density. The pixel intensity can be rendered using the volume rendering technique[13]. However,

[1]Equal Contribution.

NeRF and its variants have struggled with rendering speeds for practical deployment in real-world scenarios. Subsequent efforts along this trend introduce voxel-based implicit representation [9, 47, 51, 59, 64], hash grid [42], computational parallelism [44], or neural light field representation [56] to speed up the rendering. However, they either require task-specific design or face a trade-off between rendering quality and efficiency, making them difficult to generalize to large-scale scenarios with practical speed. Recent progress in point-based 3D Gaussian Splatting (3D-GS) [30] has brought photo-realistic rendering quality to the real-time level, even for complex scenes. The authors propose representing the scene as explicit 3D Gaussians with specific properties to model the scene; the 2D images are efficiently rendered using a technique named *splatting*[33]. The optimal balance between speed and quality indicates a potential trend to use 3D-GS as a new representation for generating numerous large-scale scenes in digital twins and autonomous driving. However, using point-based representations inevitably introduces significant storage costs, as each point and its attributes are stored independently. For instance, 3D-GS on a typical unbounded 360 scene [5] requires more than one gigabyte, which inhibits the scalability of 3D-GS (e.g., 1.4GB on scene *Bicycle*).

In this paper, we counteract the heavy storage issue and deliver a compact representation while preserving the rendering quality. By examining the well-trained point-based representation, each scene is composed of millions of Gaussians, grown from sparse Structure from Motion (SfM) point cloud. Attributes are attached to Gaussians to model the scene's geometry and appearance. However, the significant number of Gaussians, as well as the high-degree Spherical Harmonics (SH) coefficients used for modeling scene reflection, contribute to an over-parametrized representation when fitting to the scenes. To minimize the required Gaussian number, we propose proper criteria to measure the global significance of each 3D Gaussian, in the context of its contribution for view synthesis. Gaussians with low impact on visual quality will be identified and pruned, followed by short recovery steps to be applied. Spherical harmonics (SH) coefficients, as the majority of the data, are used for modeling the view-dependent color. Compressing it directly by shrinking the higher degree harms the reflectance effect, and we propose a general distillation step enhanced by pseudo-view augmentation to harmlessly transfer the knowledge into a compact level. *VecTree Quantization* step adaptively picks "just some amount" of distinct point attributes based on the global significance, further reducing the required bitwidth of the original format.

In summary, our proposed framework, **LightGaussian**, efficiently reduces the Gaussian count (e.g., from 1.49M to 575K, Fig. 1, left), significantly reducing storage requirements from 727MB to 42MB, with minimal rendering quality decrease ($\downarrow$ 0.013 in SSIM) on the Mip-NeRF 360 datasets (Fig. 1, right). LightGaussian further improves the rendering speed to a higher level (200+ FPS) on complex scenes containing detailed backgrounds, suggesting a viable solution for broadening the application scope.

2. Related Works

Efficient 3D Scene Representations for NVS Neural radiance field (NeRF) [40] uses a multi-layer perceptron (MLP) to represent a scene, and this compact representation has brought view synthesis quality to a new stage. However, NeRF suffers from extremely slow inference challenges. Follow-ups either explore ray re-parameterizations[4, 5], explicit spatial data structures [9, 19, 29, 37, 42, 51, 63], caching and distillation [20, 26, 44, 56], or ray-based representations [2, 50] for speeding up. Still, NeRF-based methods struggle to achieve real-time rendering speed in practical large-scale scenes, which is caused by the multiple queries needed for rendering a single pixel, limiting their practical use. Recently, point-based representation, 3D Gaussian Splatting (3D-GS) [30], combining the idea of point-based rendering and splatting techniques for rendering, achieves real-time speed with comparable rendering quality to the best MLP-based renderer, Mip-NeRF 360 [5]. Although promising, the heavy storage requirement to store all attributes attached to the Gaussians often requires gigabyte-level disk space for saving a single unbounded scene, and millions of Gaussians hinder the rendering efficiency of 3D-GS.

Model Pruning and Vector Quantization Model pruning involves reducing the complexity of a neural network by eliminating non-significant parameters to maintain a balance between performance and resource utilization. Unstructured [34] and structured pruning [1, 25] remove components at weight-level and neuron (mostly channel) levels to provide a smaller network with a smaller or more efficient network architecture. The iterative magnitude pruning (IMP) method, where weights of the smallest magnitude are progressively pruned over multiple iterations, has been highly successful in lottery ticket rewinding [17, 18]. Additionally, vector quantization [54] aims to represent data with discrete entries of a learned codebook (i.e., tokens) to achieve lossy compression. In general, the mean square error (MSE) is used to find the most similar pattern in the codebook to replace the original input data vector. Previous works [10, 21, 39] have shown that learning a discrete and compact representation not only contributes to visual understanding but also improves the robustness of models. In this vein, vector quantization has been widely adopted in image synthesis [14], text-to-image generation [22], and novel view synthesis [23, 36, 63].

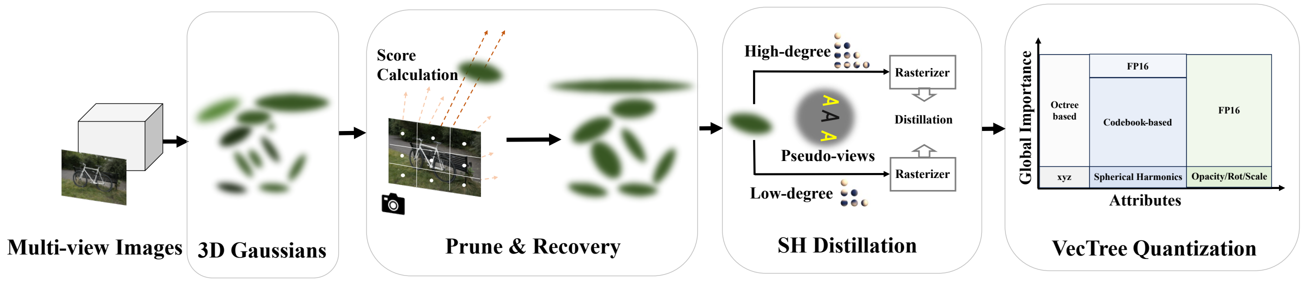

Figure 2. **The overall pipeline of LightGaussian.** 3D Gaussians are optimized from multi-view images and SfM points. LightGaussian first calculates the global significance for each Gaussian based on training observations; Gaussians with the least significance are pruned. A subsequent distillation with synthesized pseudo-views is introduced to transfer the SH into a compact format. VecTree quantization, consisting of lossy codebook quantization and lossless octree quantization, is further introduced for compressing the representation.

Knowledge Distillation Knowledge Distillation (KD) is widely adopted in various machine learning tasks [46, 49, 56, 58]. A student model is trained for the primary purpose of model compression [7] or ensembling [28] with the help of teacher models. Many variants [3, 27, 38, 45, 53, 55, 65] have been proposed to achieve better knowledge transfer from the teacher to the student models. In the field of 3D vision, neural scene representations have embraced knowledge distillation mainly through view renderings to leverage existing 2D priors. DreamFusion [43] and NeuralLift-360 [61] adopt pre-trained text-to-image diffusion models for 3D generation. DFF [32], NeRF-SOS [16], INS [15], SA3D [8] distill various pre-trained 2D image feature extractors to perform corresponding tasks in the 3D domain. Knowledge distillation has also played a key role in model compression of scene representations. R2L [56] and KiloNeRF [44] distill Neural Radiance Fields (NeRF) into more efficient representations such as light fields or multiple tiny MLPs. Our work falls into the category of utilizing knowledge distillation for model compression and leverages novel view renderings as the bridge to connect the teacher and student models.

3. Method

Overview The overview of LightGaussian is illustrated in Fig. 2. The 3D-GS model is trained using multi-view images and is initially initialized from SfM point clouds. By expanding the sparse points to millions of Gaussians, the scene is well-represented. Then, the 3D-GS undergoes processing within our pipeline to transform it into a more compact format. This involves utilizing *Gaussian Prune and Recovery* to reduce the number of Gaussians, *SH Distillation* to remove redundant SHs while preserving the modeled specular light, and *VecTree Quantization* to store Gaussians at a lower bit-width.

3.1. Background: 3D Gaussian Splatting

3D Gaussian Splatting (3D-GS) [30] is an explicit point-based 3D scene representation, utilizing Gaussians with various attributes to model the scene. When representing a complex real-world scene, 3D-GS is initialized from an SfM sparse point cloud, and *Gaussian Densifications* are applied to increase the Gaussian counts that are used for handling small-scale geometry insufficiently covered. Formally, each Gaussian is characterized by a covariance matrix $\mathbf{\Sigma}$ and a center point $\boldsymbol{X}$, which is referred to as the mean value of the Gaussian:

$$\mathrm{G}(\boldsymbol{X}) = e^{-\frac{1}{2}\boldsymbol{X}^T\mathbf{\Sigma}^{-1}\boldsymbol{X}}, \mathbf{\Sigma} = \mathbf{R}\mathbf{S}\mathbf{S}^T\mathbf{R}^T, \tag{1}$$

where $\mathbf{\Sigma}$ can be decomposed into a scaling matrix $\mathbf{S}$ and a rotation matrix $\mathbf{R}$ for differentiable optimization.

The complex directional appearance is modeled by an additional property, Spherical Harmonics (SH), with n coefficients, $\{\boldsymbol{c}_i \in \mathbb{R}^3 | i = 1, 2, \ldots, n\}$ where $n = D^2$ represents the number of coefficients of SH with degree D. A higher degree D equips 3D-GS with a better capacity to model the view-dependent effect but causes a significantly heavier attribute load.

When rendering 2D images from the 3D Gaussians, the technique of splatting [33, 62] is employed for the Gaussians within the camera planes. With a viewing transform denoted as $\boldsymbol{W}$ and the Jacobian of the affine approximation of the projective transformation represented by $\boldsymbol{J}$, the covariance matrix $\mathbf{\Sigma}'$ in camera coordinates can be computed as follows:

$$\mathbf{\Sigma}' = \boldsymbol{J}\boldsymbol{W}\mathbf{\Sigma}\boldsymbol{W}^T\boldsymbol{J}^T. \tag{2}$$

Specifically, for each pixel, the color and opacity of all the Gaussians are computed using the Gaussian's representation Eq. 1. The blending of N ordered points that overlap the pixel is given by the formula:

$$\boldsymbol{C} = \sum_{i \in N} \boldsymbol{c_i}\alpha_i \prod_{j=1}^{i-1}(1-\alpha_i). \tag{3}$$

Here, c_i, α_i represents the color and opacity of this point computed by a Gaussian with covariance $\mathbf{\Sigma}$ multiplied by an optimizable per-point opacity and SH color coefficients. In summary, each Gaussian point is characterized by attributes including: position $\boldsymbol{X} \in \mathbb{R}^3$, color defined by spherical harmonics coefficients $\boldsymbol{C} \in \mathbb{R}^{(k+1)^2} \times 3$ (where k represents the degrees of freedom), opacity $\alpha \in \mathbb{R}$, rotation factor $\boldsymbol{r} \in \mathbb{R}^4$, and scaling factor $\boldsymbol{s} \in \mathbb{R}^3$.

3.2. Gaussian Pruning & Recovery

Gaussian densification [30], which involves cloning and splitting the initial SfM point cloud, is employed to address the challenge of insufficient coverage and is used to model small-scale geometry as well as detailed scene appearance. While this strategy leads to significantly improved reconstruction quality, it results in the number of Gaussians growing from thousands to *millions* after optimization. Such an explicit point-based representation with a large number of Gaussians requires an extremely significant storage overhead. However, pruning the Gaussians based on simplistic criteria (e.g., point opacity) can lead to a substantial degradation in modeling performance, especially where the intricate scene structure may be eliminated, as is demonstrated in Fig. 3. Drawing inspiration from the success of representative neural network pruning techniques [24], which eliminate less impactful neurons without compromising the network's overall performance, we tailor a general pruning paradigm for point-based representation to reduce the over-parameterized point number in a manner that preserves the original accuracy. Therefore, identifying the most representative redundant Gaussians with recoverable accuracy is a crucial step in our approach.

Global Significance Calculation Simply relying on Gaussian opacity as a significance criterion leads to suboptimal Gaussian pruning, prompting the need for a more effective formula. Inspired by Equation 3, these 3D Gaussians can be rasterized by projecting them onto a specific camera viewpoint for image rendering. The significance of each Gaussian can then be quantified based on its contribution to each pixel across all training views, with similar principle in magnitude network pruning [35]. Consequently, we iterate over all training pixels to calculate the hit count of each Gaussian, factoring in both Gaussian opacity and volume:

$$\mathrm{GS_j} = \sum_{i=1}^{MHW} \mathbb{1}(\mathrm{G}(\boldsymbol{X}_j), r_i) \cdot \sigma_j \cdot \gamma_j(\mathbf{\Sigma}), \tag{4}$$

where j indicates the Gaussian index, and M, H, and W represent the number of training views, image height, and width, respectively. $\mathbb{1}$ is the indicator function that determines whether a Gaussian intersects with a given ray.

The use of absolute Gaussian volume tends to exaggerate the importance of background Gaussians, leading to the immoderate pruning of Gaussians that model intricate geometry. Therefore, we propose a more adaptive way to measure the dimension of its volume:

$$\gamma(\mathbf{\Sigma}) = (\mathrm{V_{norm}})^{\beta}, \tag{5}$$
$$\mathrm{V_{norm}} = \min\left(\max\left(\frac{\mathrm{V}(\mathbf{\Sigma})}{\mathrm{V_{max90}}}, 0\right), 1\right).$$

Here, the volume is firstly normalized by the 90% largest of all sorted Gaussians, clipping the range between 0 and 1, and β is introduced to provide additional flexibility.

Gaussian Co-adaptation We rank all the Gaussians based on the computed global significance scores, and provide a quantitative basis for pruning Gaussians with the lowest scores. It is worth noting that an overly aggressive pruning ratio can be detrimental to performance. Stripping away too many Gaussians can lead to a noticeable degradation in the model's accuracy and visual fidelity since incomplete scene coverage. To mitigate this, a phase of short

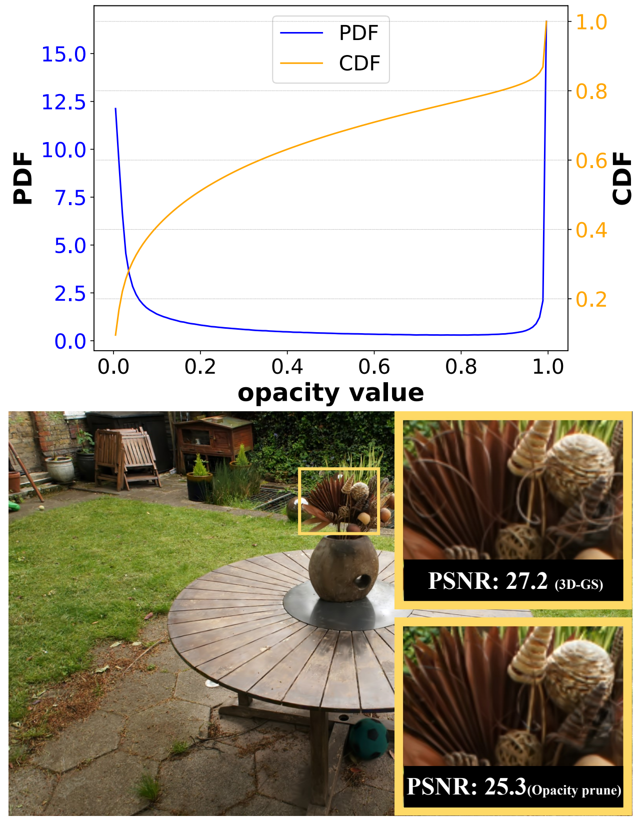

Figure 3. **Zero-shot Opacity-based Pruning**. A significant number of Gaussians exhibit small opacity values (top). Simply utilizing Gaussian opacity as an indicator for pruning the least important Gaussians results in the rendered image losing intricate details (bottom), with the PSNR dropping from 27.2 to 25.3. This has inspired us to find better criteria to measure global significance in terms of rendering quality.

Gaussian co-adaptation is essential, which involves a joint adjustment of the Gaussians' attributes, allowing them to adapt and compensate for the loss incurred by pruning.

3.3. Distilling into Compact SHs

In the uncompressed Gaussian Splat data, a significant portion is comprised of Spherical Harmonics (SH) coefficients, requiring (45+3) floating-point values per splat, which represent 81.3 percent of the total attribute volume. Reducing the degree of SH, while beneficial for decreasing disk space usage, leads to a noticeable loss of surface 'shininess', particularly affecting specular reflection variance when the viewpoint is altered.

To achieve a balance between disk storage efficiency and scene reflectance quality, we propose transferring knowledge from well-trained high-degree SHs to their compact counterparts (lower-degree) via data distillation:

$$\mathcal{L}_{\text{distill}}(\mathrm{G}_{\text{SH2-deg}}) = \frac{1}{N}\sum_{i=1}^{N} \|\boldsymbol{C}_{\text{teacher}} - \boldsymbol{C}_{\text{student}}\|_2^2. \quad (6)$$

Simply reintroducing these view-dependent visual effects to the network does not significantly enhance its knowledge. We, therefore, suggest employing the concept of data augmentation. This involves training the Gaussians not only to represent known views but also to learn behaviors from unseen (pseudo) views modeled by the teacher model, thus broadening their representational capacity.

Synthesize Pseudo Views The specular reflection rays are reflected off the surface of the light source when we move the viewpoints. We can augment the training views by sampling additional viewpoints that can reflect such reflectance. As we know the camera locations and viewing directions of all training views, we randomly sample pseudo views around each of the training views, obeying a Gaussian distribution, while fixing the camera view directions:

$$\mathbf{t}_{\text{pseudo}} = \mathbf{t}_{\text{train}} + \mathcal{N}(0, \sigma^2), \quad (7)$$

where $\mathbf{t}_{\text{pseudo}}$ and $\mathbf{t}_{\text{train}}$ represent the newly synthesized and training camera positions, respectively. $\mathcal{N}$ denotes a Gaussian distribution with mean 0 and variance σ^2, which is added to the original position to generate the new position.

3.4. VecTree Attribute Compression

Vector quantization is well-explored in voxel-based NeRF representations [36, 52, 63, 67]. Although a high compression rate can be reached, Gaussian attributes cannot be easily quantized in the same fashion. The reason is that each attribute of the explicit representation has its own physical meaning, especially when representing large-scale 3D scenes, and attributes such as opacity, rotation, and scale are more sensitive to such discretized representation, with a dramatic drop in accuracy. Therefore, we propose two ways to mitigate this gap: first, we reutilize the significance score from Sec. 3.2 and perform excessive vector quantization on the SHs of the least important Gaussians. For the Gaussian location, we draw from point cloud compression and adopt octree-based lossless compression into our framework. For the remaining important SHs and other attributes representing the Gaussian shape, rotation, and opacity, we save these features in float16 format.

Vector Quantization The codebook under vector quantization (VQ) is initialized with K codes within it, denoted as $\boldsymbol{C} = \boldsymbol{c}_1, \boldsymbol{c}_2, \boldsymbol{c}_3, \boldsymbol{c}_K$ to represent the Gaussian sets $\boldsymbol{G} = \boldsymbol{g}_1, \boldsymbol{g}_2, \boldsymbol{g}_3, \boldsymbol{g}_N$ where $K \ll N$. To assign each code to the Gaussian feature, we randomly select a batch of Gaussians at each iteration and calculate the Euclidean distance between the selected Gaussian and each code vector in the codebook to determine which code the Gaussian is associated with. Then, a significance-weighted codebook optimization is applied: $\mathbf{c}_i := \lambda \cdot \mathbf{c}_i + (1-\lambda) \cdot \sum \mathbf{g}_j \in \mathcal{R}(\mathbf{c}_k)\mathrm{GS}_j \cdot \mathbf{g}_j$, where $\mathbf{g}_j \in \mathcal{R}(\mathbf{c}_i)$ denotes the j-th Gaussian assigned to the i-th code, and λ controls the contribution from the moving average. We only perform excessive VQ on the least 60% of Gaussians, since we are representing complex, large-scale scenes.

Octree-based Compression Unstructured and high-precision 3D points pose a challenge for efficient storage, especially for large-scale scenes. Applying lossy compression to Gaussian locations shows significant rendering degradation, as the Gaussian location is sensitive to the subsequent rasterization accuracy. Therefore, drawing from the Point Cloud Compression literature [48], which applies lossless encoding on the Gaussian location, utilizing the octree geometry codec in G-PCC [41] consumes only a very small amount of bits. Specifically, let $(X_i = (x_i, y_i, z_i))_{i=1\ldots N}$ be the set of 3D positions associated with the points of the input point cloud. The L-PCC encoder [48] computes the quantized positions $(\hat{X}_i)_{i=1\ldots N}$ as follows: $\hat{X}_i = \lfloor (X_i - X_{shift}) \times s \rfloor$, where X_{shift} and s are predefined parameters and we set all octree-related parameters the same as PCGCv2 [57].

For the decoding stage, the reconstructed positions $(\hat{X}_i)_{i=1}^{N}$ are generated by applying the following inverse quantization process: $\hat{X}_i = \frac{\hat{X}i}{s} + X_{shift}$.

4. Experiments

4.1. Experimental Settings

Datasets and Metrics Comparisons are performed on the widely adopted scene-scale view synthesis data created by Mip-NeRF360 [6], which contains nine real-world large-scale scenes (5 unbounded outdoors, 4 indoors with detailed backgrounds). We utilize the published seven

Methods	Mip-NeRF 360 Datasets					Tank and Temple Datasets				
	FPS↑	Size↓	PSNR↑	SSIM↑	LPIPS↓	FPS↑	Size↓	PSNR↑	SSIM↑	LPIPS↓
Plenoxels [64]	6.79	2100MB	23.62	0.670	0.443	11.2	2700MB	21.07	0.719	0.379
INGP-Big [42]	9.43	48MB	26.75	0.751	0.299	2.79	48MB	21.92	0.744	0.305
Mip-NeRF 360 [5]	0.06	8.6MB	29.23	0.844	0.207	0.09	8.6MB	22.21	0.759	0.257
VQ-DVGO [36]	6.53	56.07MB	25.44	0.699	0.325	-	-	-	-	-
3D-GS [30]	139	727MB	29.13	0.870	0.185	106	380MB	23.11	0.822	0.219
Ours	215	42.48MB	28.45	0.857	0.210	209	22.43MB	22.83	0.807	0.242

Table 1. **Quantitative Comparisons in Real-world Large-scale Scenes.** We compare LightGaussian with the original 3D-GS [30], efficient voxel-based NeRFs [42, 64], voxel NeRF with vector quantization [36], and compact MLP-based NeRF [5]. Voxel-based methods all exhibit a lack of sufficient capacity for representing large-scale scenes and are not able to run at real-time speed. Mip-NeRF 360 produces the best visual quality, but it requires more than 16s to render a single image. Our method achieves a good balance among FPS, model size, and rendering quality.

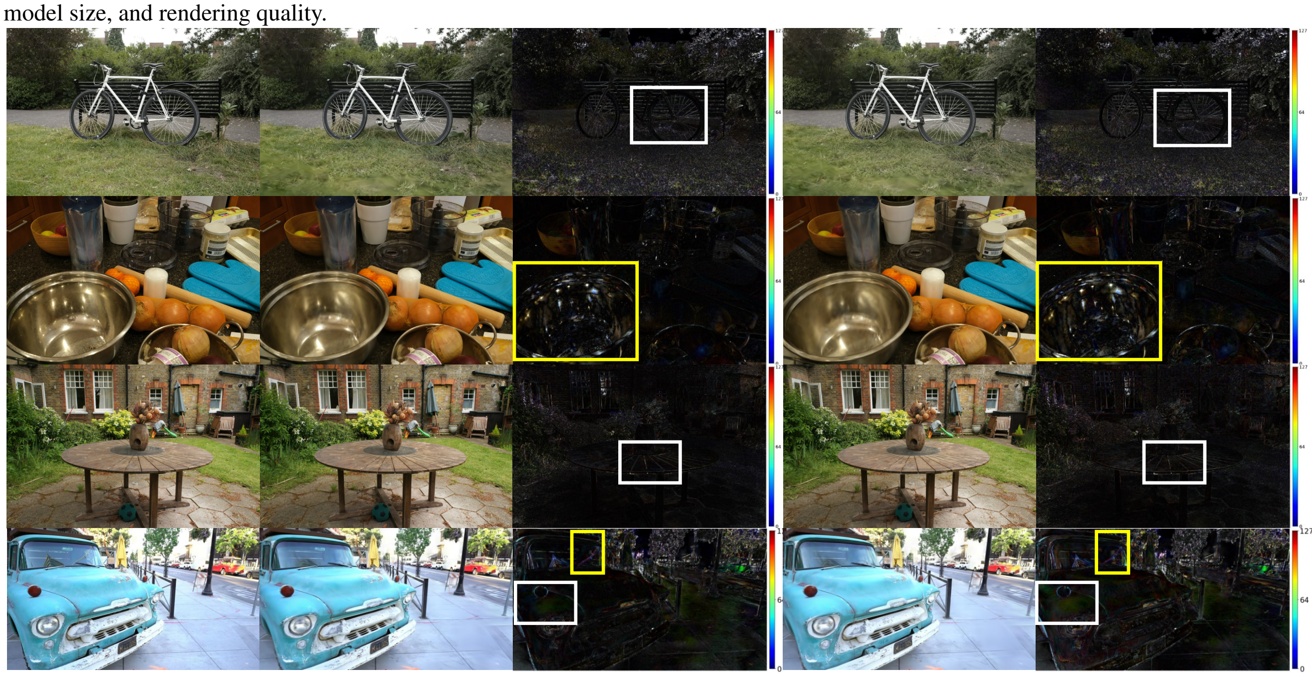

Ground-truth RGB (3D-GS) Residual Map (3D-GS) RGB (Ours) Residual Map (Ours)

Figure 4. **Visual Comparisons**. We compare LightGaussian with the vanilla 3D-GS [30], presenting a residual map between prediction and ground-truth scaled from 0 to 127 to highlight the differences. We observe that LightGaussian preserves the specular reflections (yellow boxes) after converting to a compact format. Additionally, a slight lightness change is noted after the conversion, as shown in the bottom white box. For dynamic viewpoint comparisons, please refer to our supplementary video material.

scenes for comparison following the train/test split in Mip-NeRF360 [6]. Additionally, we use another large-scale unbounded dataset, the Tanks and Temples dataset [31], where we perform comparisons using the same two scenes as used in 3D-GS [30]. In total, the adopted datasets consist of scenes with very different capture styles and cover both bounded indoor scenes with detailed backgrounds and large unbounded outdoor cases. The rendering quality is reported using metrics such as peak signal-to-noise ratio (PSNR), structural similarity (SSIM), and perceptual similarity via LPIPS [66].

Compared Baselines We compare with methods that can model large-scale scenes, including Plenoxel [64], Mip-NeRF360 [5], and 3D-GS [30], along with representative efficient methods such as Instant-ngp [42], which uses a hash grid for storage, and VQ-DVGO [36], utilizing DVGO [51] as the basic representation and introducing voxel pruning and vector quantization to it.

Implementation Details The framework is developed using Pytorch and reuses the differential Gaussian rasterization presented by 3D-GS [30]. We use our own trained checkpoints that match performance with those detailed in the 3D-GS paper [30]. For the *Global Significance Calculation*, we set the power to 0.1 in Eq. 5, and fine-tune for 5,000 steps in Gaussian Co-adaptation. For the *SHs Distillation*, we reduce the 3-degree SHs to 2-degree, eliminating 21 elements for each Gaussian, and enhance it with σ set to 0.1 in the pseudo view synthesis. For the *VecTree Compression*,

Exp#	Model	FPS↑	Size↓	PSNR↑	SSIM↑	LPIPS↓
[1]	Baseline (3D-GS [30])	192.05	353MB	31.68	0.926	0.200
[2]	+ Gaussian Pruning.	312.30	116MB	30.32	0.911	0.222
[3]	+ Co-adaptation	303.99	116MB	31.85	0.925	0.206
[4]	+ SH Compactness.	318.97	77MB	30.54	0.914	0.217
[5]	+ Distillation	304.20	77MB	31.47	0.922	0.211
[6]	+ Pseudo-views	300.60	77MB	31.59	0.923	0.211
[7]	+ Codebook Quant.	300.60	23MB	31.26	0.917	0.220
[8]	+ Octree Compression.	300.60	20MB	31.26	0.917	0.220
[9]	LightGaussian (Ours)	300.60	20MB	31.26	0.917	0.220

Table 2. Ablation studies on the *Gaussian Pruning*, *SH Compactness*, and the *VecTree Compression*. Scene: **Room**. Zero-shot Gaussian pruning leads to a degradation in rendering quality (#2), but Co-adaptation can recover most of the scene details (#3). Directly eliminating high-order SH negatively affects the quality (#4), while distillation with pseudo-view helps to mitigate the gap (#5, #6). Codebook quantization significantly reduces the required model size (#7), while lossless Octree compression helps to preserve the overall quality.

Model	FPS↑	Size↓	PSNR↑	SSIM↑	LPIPS↓
Baseline	192.05	353MB	31.68	0.926	0.200
Hit Count Only	300.57	116MB	28.28	0.895	0.238
× Opacity.	310.29	116MB	30.10	0.910	0.222
× Opacity × γ(Volume).	312.30	116MB	30.32	0.911	0.222
+ Co-adaptation	303.99	116MB	31.85	0.925	0.206

Table 3. Ablation study of the *Gaussian Pruning*, by using different Gaussian attributes for computing its global significance score. By considering only the hit count of each Gaussian from training rays, the zero-shot pruning leads to inferior performance. Incorporating the opacity and volume drives us to a better criterion. The subsequent Gaussian Co-adaptation is used to recover most of the information loss from the pruning of redundant Gaussians.

Model	Size↓	PSNR↑	SSIM↑	LPIPS↓
Baseline	77.09MB	31.59	0.923	0.211
+FP16	36.76MB	31.58	0.923	0.212
+ VQ All att.	18.58MB	22.97	0.750	0.378
+ VQ All att. × GS	18.58MB	26.39	0.830	0.327
+ VQ SH.	22.53MB	30.94	0.910	0.225
+ VQ SH × GS	22.53MB	31.26	0.917	0.220
VecTree	20.65MB	31.26	0.917	0.220

Table 4. Ablation study of hybrid *VecTree Quantization* (VQ). By quantizing all attributes to FP16, except for Gaussian locations due to their sensitivity, a smaller model is achieved. VQ is applied to all attributes leads to inferior modeling accuracy, but this can be mitigated by using Global Significance (GS) on the least crucial Gaussians. Other attributes (e.g., scale) are also sensitive to VQ, hence we only apply VQ on the SH. Combining this with Octree compression results in our VecTree Compression (the last row), which demonstrates a good balance between size and quality.

we set the codebook size to 8192.

4.2. Experimental Results

Quantitative Results To assess the quality and model size of different methods for novel view synthesis, we summarize the quantitative numbers in Tab. A6, including highly efficient voxel-based NeRFs (Plenoxel[64], Instant-NGP [42]), the compact MLP-based Mip-NeRF360 [5], NeRF with vector quantization [36], and 3D Gaussian Splatting [30]. Specifically, in the Mip-NeRF360 datasets, the NeRF-based methods, benefiting from their compact representation by using MLPs, show competitive accuracy, but the slow inference speed (0.06FPS) makes them impractical for real-world applications. Voxel-based NeRFs partly resolve the rendering efficiency issue, but the FPS still lags behind for practical usage, while Plenoxel requires 2.1GB for storing a large-scale scene. VQ-DVGO optimizes the storage issue, but their pruning and purely vector quantization make it challenging to generalize to complex large-scale scenes. On the other hand, 3D-GS strikes a balance in rendering quality and real-time rendering speed; however, it requires nearly gigabytes for storing a single scene. Our pipeline, LightGaussian, achieves the fastest rendering speed (1.55×) compared to all existing methods, thanks to its pruning of insignificant Gaussians for an efficient rasterization process. Moreover, the compact SH representation and VecTree compression further reduce the model redundancy in 3D Gaussians, shrinking the model size from 727MB to 42.48MB on Mip-NeRF360 datasets, a 17× reduction ratio. LightGaussian also achieves nearly 2× faster rendering speed on the Tank & Temple datasets, while reducing the storage from 380MB to 22.43MB.

Qualitative Results We compare the rendering result of all adopted baselines, with the highlight on intricate details and the background regions in Fig. 4. We can observe Mip-NeRF360, 3D-GS and our LightGaussian achieves the best visual quality, whereas Mip-NeRF360 requires more than 30 seconds to render an image of resolution 1080p, 3D-GS requires 17× times more disk storage requirement.

4.3. Ablation Studies

We ablate components of our method by separately analyzing the proposed modules. Specifically, we find that *Iterative Gaussian Pruning* is effective in removing redundant Gaussians, *SHs Distillation* effectively reduces the SH's degree, and *Vector Quantization* efficiently compresses the feature space, leading to a more compact and efficient rep-

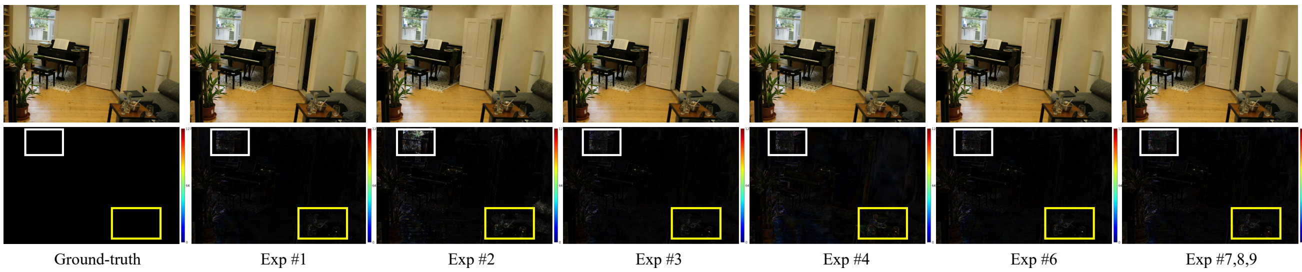

Figure 5. **Visual Comparisons for Ablation Study**. We visualize the rendered RGB images and the residual map between the ground-truth image, aligned with the experiment ID as shown in Tab. 2. The final model (Exp #7, #8, #9) demonstrates close results to 3D-GS (Exp #1), while the Gaussian Co-adaptation, along with SH distillation, almost completely mitigates the information loss.

resentation. These individual contributions collectively enhance the overall performance of our framework.

Overall Analysis We report the performance of the investigation on the proposed modules in Tab. 2 and Fig. 5. We verify that our design of *Gaussian Pruning & Recovery* is effective in removing redundant Gaussians (Exp #1→3) with negligible quality degradation while preserving rendering accuracy. This proves that the proposed Global Significance, based on Gaussian attributes, accurately represents the critical aspects. By removing the high-degree SHs and transferring the knowledge to a compact representation (Exp #3 →5), our method successfully demonstrates the benefits from using soft targets and extra data from view augmentation, results in negligible changes in specular reflection In practical post-processing, the vector quantization on the least important Gaussians (Exp #7), combined with the octree-based lossless compression for its geometric position (Exp #8), showcases the advantage of adopting a hybrid compression.

The Best Significance Criteria? To discover the most favorable criteria to measure the global significance of each Gaussian, we study the critical elements within each Gaussian, including its hit count with all training rays, Gaussian opacity, and the function-related volume. As shown in Tab. 3, considering all these three attributes by weighting the hit count using opacity and Gaussian volume produces the most accurate rendering quality after zero-shot pruning. A brief Gaussian Co-adaptation (last row) could restore accuracy to its level prior to pruning. We visualize the rasterized images before and after pruning, as well as the pruned Gaussians, in Fig. 6.

SH Distillation Directly eliminating the high-degree component of SHs leads to an unacceptable performance drop from the full model (Exp #3 → 4), where we can also observe a significant loss of specular reflection on surfaces when changing viewpoints. However, by introducing knowledge distillation (Exp #4 → 5) from the full model, we can reduce its size and preserve the viewing effects. Additionally, adding pseudo-views during training (Exp #5 → 6) further demonstrates the effectiveness of guiding the training of a student model through the teacher model.

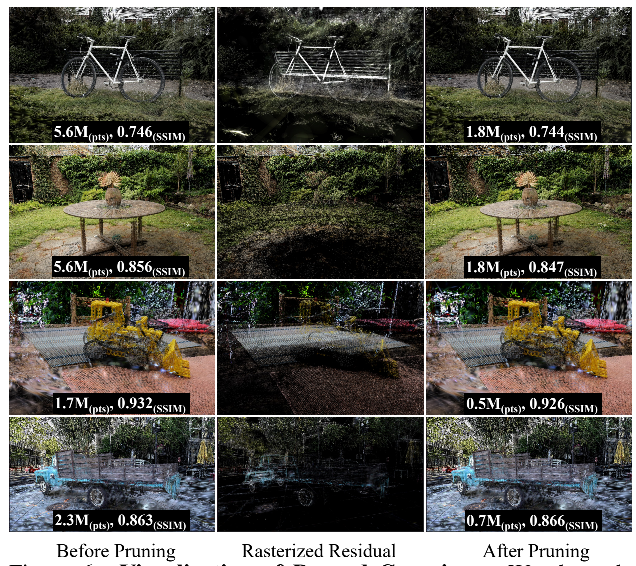

Figure 6. **Visualization of Pruned Gaussians**. We show the pruned Gaussians (middle) obtained by applying the proposed *Gaussian Prune and Recovery*. The residual is visualized by rasterizing the pruned Gaussians.

VecTree Attribute Compression We study the effectiveness of applying quantization on Gaussian attributes, as shown in Tab. 4. We find that the Gaussian location is sensitive to a low-bit representation and thus apply lossless Octree-based compression on it. For the rest of the attributes, we first quantize them to half-precision, and applying Vector Quantization (VQ) on all attributes leads to inferior results, but this can be mitigated by using Gaussian Global Significance. The final module, VecTree Compression, performs Octree-based compression on Gaussian location, VQ on the least important SHs, and FP16 on the rest, achieving the best performance balance.

5. Conclusion

We present LightGaussian, a novel framework that converts the heavy point-based representation into a compact format for efficient novel view synthesis. For practical use, LightGaussian explores the use of 3D Gaussians for modeling large-scale scenes and finds an effective way to identify the least important Gaussians grown by densification. In pursuing a compact Spherical Harmonics format, distillation is enhanced by synthesizing pseudo-views to generate more data for knowledge transfer. A VecTree compression post-processing effectively removes further redundancy by using Gaussian significance as an indicator. With these methods, the proposed representation reduces data redundancy by more than 15×, further boosting the FPS to more than 200 FPS, with minimal rendering quality loss.

A6. More Technical Details

We detail the procedures of LightGaussian in Algorithm 1. The trained 3D-GS [30] features a Gaussian location with a dimension of 3, Spherical Harmonics coefficients with a dimension of 48, and opacity, rotation, and scale, whose dimensions are 1, 4, and 3, respectively.

Algorithm 1 The overall pipeline of LightGaussian

Initialize: Training view images $\mathcal{I} = \{\boldsymbol{I}_i \in \mathbb{R}^M\}_{i=1}^N$ and their associated camera poses $\mathcal{P} = \{\boldsymbol{\phi}_i \in \mathbb{R}^{3\times 4}\}_{i=1}^N$.

Pre-Training 3D-GS [30].
$\boldsymbol{G}_i$ with attributes XYZ, SH-3deg, Opacity, Rotation, Scale.
#Gaussian Pruning and Recovery.
$\mathcal{G} = \{\boldsymbol{G}_i \in \mathbb{R}^{(3+48+1+4+3)})\}_{i=1}^N \leftarrow$ 3D-GS$(\mathcal{I}, \mathcal{P})$
$\mathcal{G} \leftarrow$ CALGS$(\mathcal{G}, \mathcal{P})$ ▷ Assign Global Significance
$\hat{\mathcal{G}} \leftarrow$ PRUNE$(\mathcal{G})$ ▷ Prune Least Significant Ones
$\hat{\mathcal{G}} \leftarrow$ RECOVERY$(\hat{\mathcal{G}})$ ▷ Gaussian Recovery
#Distilling into Compact SHs.
SH-2deg $\leftarrow$ REDUCESH(SH-3deg) ▷ Reduce the SH degree
while Few Steps **do** ▷ SH Distillation
  $\hat{\mathcal{P}}$ = SampleView$(\mathcal{P})$ ▷ Synthesize Pseudo Views
  $I_t \leftarrow$ TEACHER$(\hat{\mathcal{P}})$ ▷ Teacher render
  $I_s \leftarrow$ STUDENT$(\hat{\mathcal{P}})$ ▷ Student render
  $\nabla L \leftarrow$ LOSS(I_s, I_t)
  $\hat{\mathcal{G}} \leftarrow$ ADAM(∇L) ▷ Backprop & Step
end while
#VecTree Quantization.
SH-2Deg-VQ $\leftarrow$ VECTORQUANTIZATION(SH-2Deg, $\hat{\mathcal{G}}$)
$\hat{\mathcal{G}}$-fp16 $\leftarrow$ CONVERTTOFLOAT16$(\hat{\mathcal{G}})$
XYZ$'$ $\leftarrow$ OCTREECOMPRESSION(XYZ)
#Save Model.
Save optimized model $\hat{\mathcal{G}}$ to disk.

Specifically, we describe how we calculate the Global Significance Score for each trained Gaussian in Algorithm 2.

Algorithm 2 Global significance calculation for gaussians.

$\mathcal{G}$ contains all gaussians with attributes XYZ, SH-3deg, Opacity, Rotation, Scale.
$\mathcal{P}$ Sample Camera poses from training.
function $CalGS(\mathcal{G}, \mathcal{P})$
  $GS \leftarrow 0$ ▷ Init Global Significance
  for all pixels i in renderFunc$(\mathcal{P})$ **do**
    $H \leftarrow$ GETHITCOUNT$(\mathcal{G}, i)$ ▷ Gaussian Hit count
    # Eq.5 in the main draft.
    $GS \leftarrow GS + H \cdot Opacity^{\intercal} \cdot$ VNORM$(Scale)^{\intercal}$
  end for
  return GS
end function

A7. More Experiment Results

In addition to realistic indoor and outdoor scenes in the Mip-NeRF360 [5] and Tank and Temple datasets [31], we further evaluate our method on the synthetic *Blender* dataset [40], and provide a scene-wise evaluation on all datasets, accompanied by detailed visualizations.

Results on NeRF-Synthetic 360°(Blender) Dataset. The synthetic *Blender* dataset [40] includes eight photo-realistic synthetic objects with ground-truth controlled camera poses and rendered viewpoints (100 for training and 200 for testing). Similar to 3D-GS [30], we start training the model using random initialization. Consequently, we calculate the Global Significance of each Gaussian, work to reduce the SH redundancy, and apply the VecTree Compression (codebook size set at 8192) to the learned representation. Overall comparisons with previous methods are listed in Table A5, where we observe our LightGaussian markedly reduces the average storage size from 52.38MB to 7.89MB, while improving the FPS from 310 to 411 with only a slight rendering quality decrease.

Additional Qualitative Results on Mip-NeRF360. We provide extra visualizations for 3D-GS [30], LightGaussian (ours), and VQ-DVGO [36], accompanied by the corresponding residual maps from the ground truth. As evidenced in Figure A7 and Figure A8, LightGaussian outperforms VQ-DVGO, which utilizes NeRF as a basic representation. Furthermore, LightGaussian achieves a comparable rendering quality to 3D-GS [30], demonstrating the effectiveness of our proposed compact representation.

Additional Quantitative Results on Mip-NeRF360. Tables A6, A7, and A8 present the comprehensive error metrics compiled for our evaluation across all real-world scenes (Mip-NeRF360 and Tank and Temple datasets). Our method not only compresses the average model size from

Table A5. **Per-scene results on Synthetic-NeRF.**

Method	Chair	Drums	Ficus	Hotdog	Lego	Materials	Mic	Ship	Avg.
					Size(MB)				
3D-GS	94.612	64.163	35.839	39.607	64.910	29.335	34.185	56.400	52.381
Ours	13.785	9.596	5.473	5.994	9.600	4.542	5.252	8.464	7.838
					PSNR(dB)				
3D-GS	35.436	26.294	35.614	37.848	35.782	30.533	36.585	31.642	33.716
Ours	34.769	26.022	34.484	36.461	34.944	29.341	35.370	30.405	32.725
					SSIM				
3D-GS	0.987	0.954	0.987	0.985	0.981	0.961	0.992	0.904	0.969
Ours	0.986	0.952	0.985	0.982	0.979	0.954	0.990	0.896	0.965
					LPIPS				
3D-GS	0.0133	0.0405	0.0121	0.0232	0.0195	0.0404	0.0073	0.111	0.0334
Ours	0.0142	0.0431	0.0137	0.0275	0.0222	0.0461	0.0087	0.121	0.0370

727MB to 42MB, but also consistently demonstrates comparable metrics with 3D-GS on all scenes. LightGaussian additionally shows better rendering quality than Plenoxel, INGP, mip-NeRF360, and VQ-DVGO.

Implementation Details of VQ-DVGO. In the implementation of VQ-DVGO [36], we initially obtain a non-compressed grid model following the default training configuration of DVGO [51]. The pruning quantile β_p is set to 0.001, the keeping quantile β_k is set to 0.9999, and the codebook size is configured to 4096. We save the volume density and the non-VQ voxels in the fp16 format without additional quantization. For the joint finetuning process, we have increased the iteration count to 25,000, surpassing the default setting of 10,000 iterations, to maximize the model's capabilities. All other parameters are aligned with those specified in the original VQ-DVGO paper [36], ensuring a faithful replication of established methodologies.

Table A6. **Quantitative Comparison (PSNR) for Mip-NeRF360 and Tank & Temple Scenes.**

Methods	PSNR								
	bicycle	garden	stump	room	counter	kitchen	bonsai	truck(T&T)	train(T&T)
Plenoxels	21.912	23.4947	20.661	27.594	23.624	23.420	24.669	23.221	18.927
INGP-Big	22.171	25.069	23.466	29.690	26.691	29.479	30.685	23.383	20.456
mip-NeRF360	24.305	26.875	26.175	31.467	29.447	31.989	33.397	24.912	19.523
VQ-DVGO	22.089	24.119	23.455	28.423	26.084	25.930	27.985	-	-
3D-GS	25.122	27.294	26.783	31.687	29.114	31.618	32.307	24.778	21.449
Ours	24.960	26.735	26.701	31.271	28.113	30.402	31.014	24.561	21.095

Table A7. **Quantitative Comparison (SSIM) for Mip-NeRF360 and Tank & Temple Scenes.**

Methods	SSIM								
	bicycle	garden	stump	room	counter	kitchen	bonsai	truck(T&T)	train(T&T)
Plenoxels	0.496	0.6063	0.523	0.8417	0.759	0.648	0.814	0.774	0.663
INGP-Big	0.512	0.701	0.594	0.871	0.817	0.858	0.906	0.800	0.689
mip-NeRF360	0.685	0.809	0.745	0.910	0.892	0.917	0.938	0.857	0.660
VQ-DVGO	0.473	0.613	0.564	0.860	0.777	0.763	0.842	-	-
3D-GS	0.746	0.856	0.770	0.914	0.914	0.932	0.946	0.863	0.781
Ours	0.738	0.836	0.768	0.926	0.893	0.914	0.933	0.855	0.760

Table A8. **Quantitative Comparison (LPIPS) for Mip-NeRF360 and Tank & Temple Scenes.**

Methods	LPIPS								
	bicycle	garden	stump	room	counter	kitchen	bonsai	truck(T&T)	train(T&T)
Plenoxels	0.506	0.3864	0.503	0.4186	0.441	0.447	0.398	0.335	0.422
INGP-Big	0.446	0.257	0.421	0.261	0.306	0.195	0.205	0.249	0.360
mip-NeRF360	0.305	0.171	0.265	0.213	0.207	0.128	0.179	0.159	0.354
VQ-DVGO	0.572	0.404	0.424	0.219	0.244	0.219	0.191	-	-
3D-GS	0.245	0.122	0.242	0.200	0.186	0.118	0.184	0.175	0.262
Ours	0.265	0.155	0.261	0.220	0.218	0.147	0.204	0.188	0.296

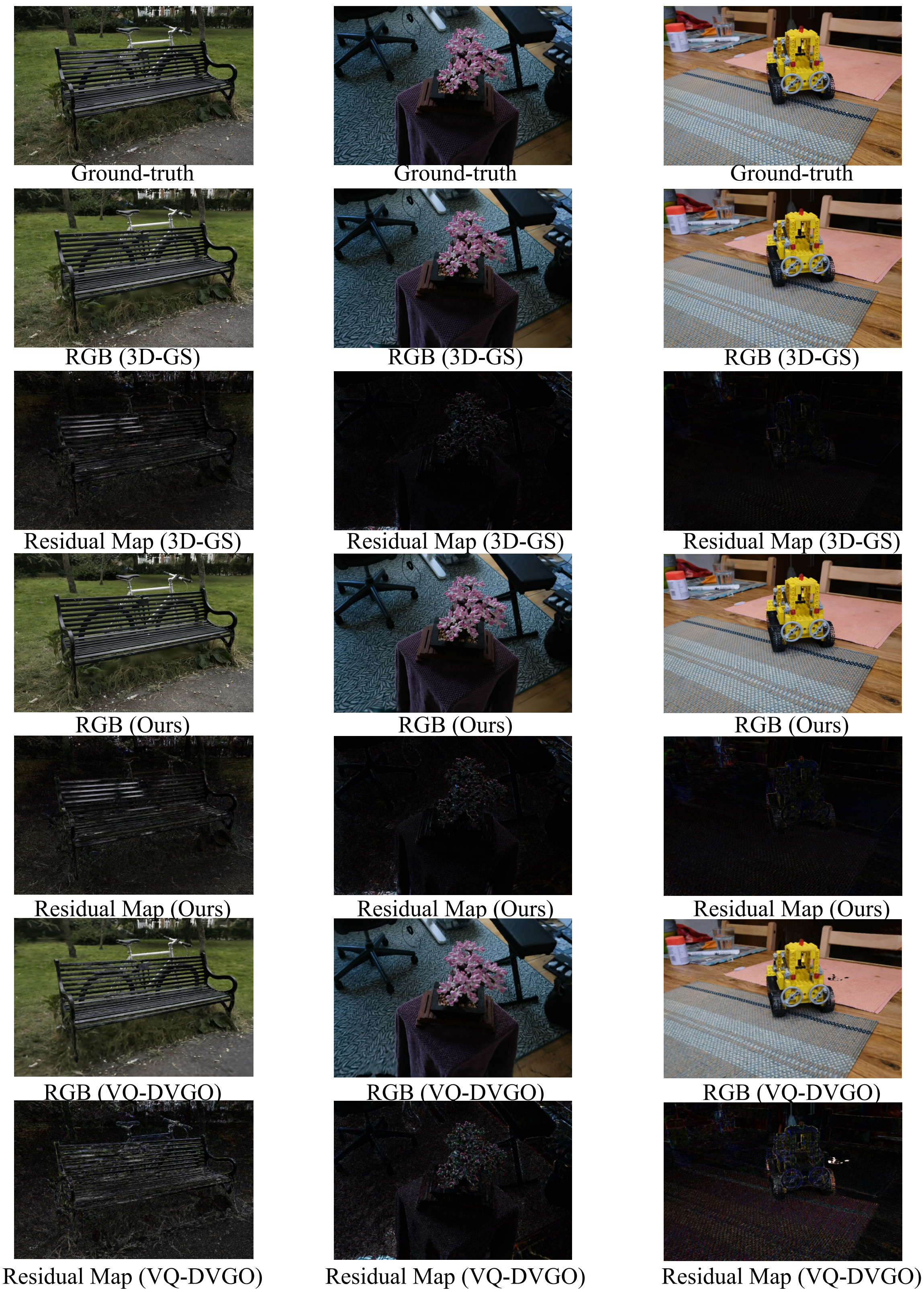

Figure A7. **Additional Visual Comparisons on the Mip-NeRF360 Datasets**. We present the rendering results from 3D-GS [30], Light-Gaussian, and VQ-DVGO [36]. The corresponding residual maps highlighting the differences between the rendered images and ground truth (GT) images are also displayed.

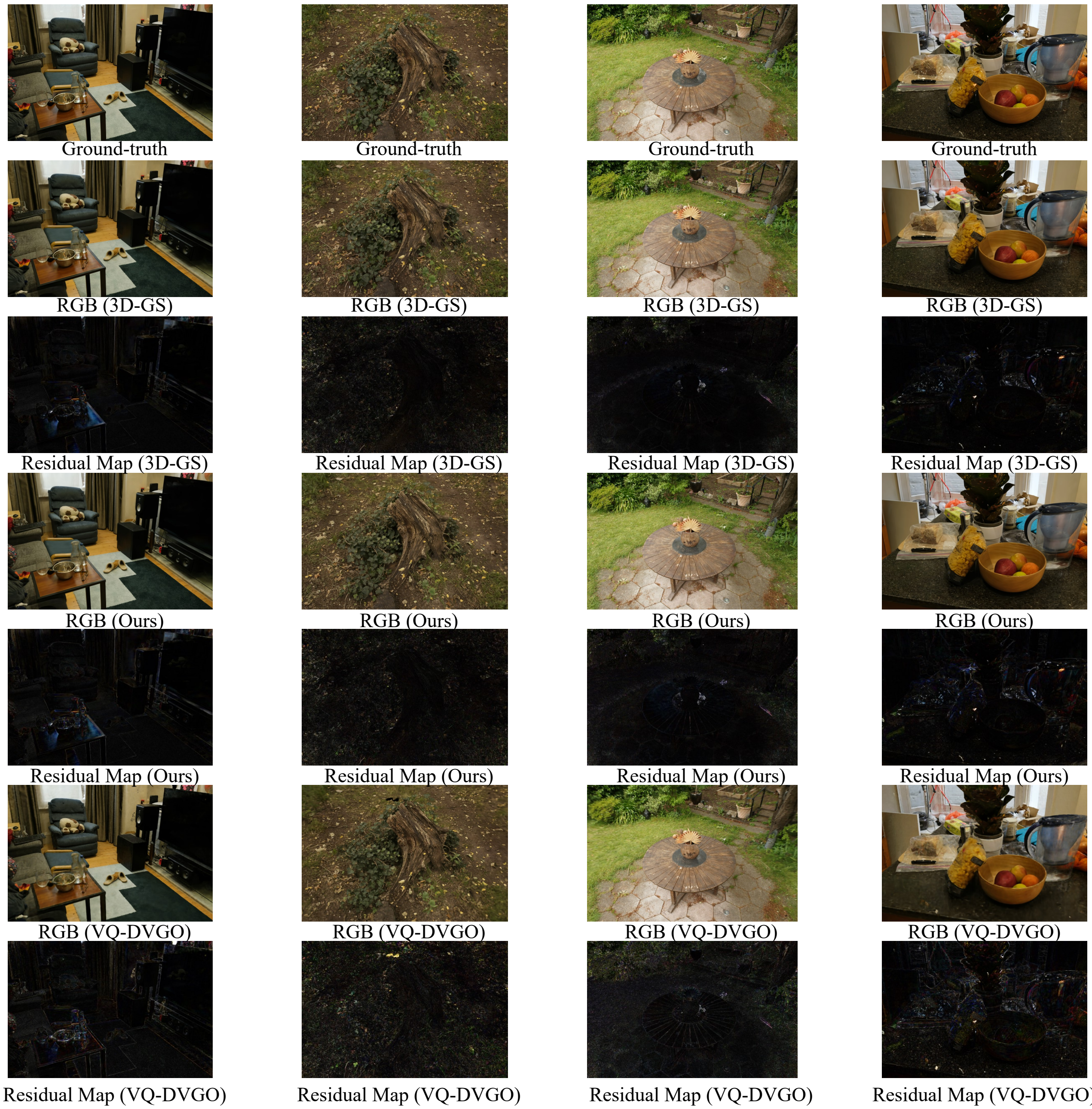

Figure A8. **Additional Visual Comparisons on the Mip-NeRF360 Datasets**. We present the rendering results from 3D-GS [30], Light-Gaussian, and VQ-DVGO [36]. The corresponding residual maps highlighting the differences between the rendered images and ground truth (GT) images are also displayed.

References

[1] Sajid Anwar, Kyuyeon Hwang, and Wonyong Sung. Structured pruning of deep convolutional neural networks. *ACM Journal on Emerging Technologies in Computing Systems (JETC)*, 13(3):1–18, 2017. 2

[2] Benjamin Attal, Jia-Bin Huang, Michael Zollhoefer, Johannes Kopf, and Changil Kim. Learning Neural Light Fields With Ray-Space Embedding Networks. *2022 IEEE/CVF Conference on Computer Vision and Pattern Recognition (CVPR)*, pages 19787–19797, 2022. 2

[3] Jimmy Ba and Rich Caruana. Do deep nets really need to be deep? *Advances in neural information processing systems*, 27, 2014. 3

[4] Jonathan T Barron, Ben Mildenhall, Matthew Tancik, Peter Hedman, Ricardo Martin-Brualla, and Pratul P Srinivasan. Mip-Nerf: A Multiscale Representation for Anti-Aliasing Neural Radiance Fields. In *Proceedings of the IEEE/CVF International Conference on Computer Vision*, pages 5855–5864, 2021. 1, 2

[5] Jonathan T. Barron, Ben Mildenhall, Dor Verbin, Pratul P. Srinivasan, and Peter Hedman. Mip-NeRF 360: Unbounded Anti-Aliased Neural Radiance Fields. *2022 IEEE/CVF Conference on Computer Vision and Pattern Recognition (CVPR)*, pages 5460–5469, 2022. 1, 2, 6, 7, A9

[6] Jonathan T Barron, Ben Mildenhall, Dor Verbin, Pratul P Srinivasan, and Peter Hedman. Mip-nerf 360: Unbounded anti-aliased neural radiance fields. In *Proceedings of the IEEE/CVF Conference on Computer Vision and Pattern Recognition*, pages 5470–5479, 2022. 5, 6

[7] Cristian Buciluǎ, Rich Caruana, and Alexandru Niculescu-Mizil. Model compression. In *Proceedings of the 12th ACM SIGKDD international conference on Knowledge discovery and data mining*, pages 535–541, 2006. 3

[8] Jiazhong Cen, Zanwei Zhou, Jiemin Fang, Wei Shen, Lingxi Xie, Xiaopeng Zhang, and Qi Tian. Segment anything in 3d with nerfs. *arXiv preprint arXiv:2304.12308*, 2023. 3

[9] Anpei Chen, Zexiang Xu, Andreas Geiger, Jingyi Yu, and Hao Su. Tensorf: Tensorial radiance fields. In *European Conference on Computer Vision*, pages 333–350. Springer, 2022. 2

[10] Gabriella Csurka, Christopher Dance, Lixin Fan, Jutta Willamowski, and Cédric Bray. Visual categorization with bags of keypoints. In *Workshop on statistical learning in computer vision, ECCV*, pages 1–2. Prague, 2004. 2

[11] Jianmei Dai, Zhilong Zhang, Shiwen Mao, and Danpu Liu. A view synthesis-based 360° vr caching system over mec-enabled c-ran. *IEEE Transactions on Circuits and Systems for Video Technology*, 30(10):3843–3855, 2019. 1

[12] Luca De Luigi, Damiano Bolognini, Federico Domeniconi, Daniele De Gregorio, Matteo Poggi, and Luigi Di Stefano. Scannerf: a scalable benchmark for neural radiance fields. In *Proceedings of the IEEE/CVF Winter Conference on Applications of Computer Vision*, pages 816–825, 2023. 1

[13] Robert A Drebin, Loren Carpenter, and Pat Hanrahan. Volume rendering. *ACM Siggraph Computer Graphics*, 22(4): 65–74, 1988. 1

[14] Patrick Esser, Robin Rombach, and Bjorn Ommer. Taming transformers for high-resolution image synthesis. In *Proceedings of the IEEE/CVF conference on computer vision and pattern recognition*, pages 12873–12883, 2021. 2

[15] Zhiwen Fan, Yifan Jiang, Peihao Wang, Xinyu Gong, Dejia Xu, and Zhangyang Wang. Unified implicit neural stylization. In *European Conference on Computer Vision*, pages 636–654. Springer, 2022. 3

[16] Zhiwen Fan, Peihao Wang, Yifan Jiang, Xinyu Gong, Dejia Xu, and Zhangyang Wang. Nerf-sos: Any-view self-supervised object segmentation on complex scenes. *arXiv preprint arXiv:2209.08776*, 2022. 3

[17] Jonathan Frankle and Michael Carbin. The lottery ticket hypothesis: Finding sparse, trainable neural networks. *arXiv preprint arXiv:1803.03635*, 2018. 2

[18] Jonathan Frankle, Gintare Karolina Dziugaite, Daniel Roy, and Michael Carbin. Linear mode connectivity and the lottery ticket hypothesis. In *International Conference on Machine Learning*, pages 3259–3269. PMLR, 2020. 2

[19] Sara Fridovich-Keil, Alex Yu, Matthew Tancik, Qinhong Chen, Benjamin Recht, and Angjoo Kanazawa. Plenoxels: Radiance Fields Without Neural Networks. In *Proceedings of the IEEE/CVF Conference on Computer Vision and Pattern Recognition*, pages 5501–5510, 2022. 2

[20] Stephan J Garbin, Marek Kowalski, Matthew Johnson, Jamie Shotton, and Julien Valentin. Fastnerf: High-fidelity neural rendering at 200fps. In *Proceedings of the IEEE/CVF International Conference on Computer Vision*, pages 14346–14355, 2021. 2

[21] Robert Gray. Vector quantization. *IEEE Assp Magazine*, 1 (2):4–29, 1984. 2

[22] Shuyang Gu, Dong Chen, Jianmin Bao, Fang Wen, Bo Zhang, Dongdong Chen, Lu Yuan, and Baining Guo. Vector quantized diffusion model for text-to-image synthesis. In *Proceedings of the IEEE/CVF Conference on Computer Vision and Pattern Recognition*, pages 10696–10706, 2022. 2

[23] Haoyu Guo, Sida Peng, Yunzhi Yan, Linzhan Mou, Yujun Shen, Hujun Bao, and Xiaowei Zhou. Compact neural volumetric video representations with dynamic codebooks. In *Thirty-seventh Conference on Neural Information Processing Systems*, 2023. 2

[24] Song Han, Jeff Pool, John Tran, and William Dally. Learning both weights and connections for efficient neural network. *Advances in neural information processing systems*, 28, 2015. 4

[25] Yang He, Guoliang Kang, Xuanyi Dong, Yanwei Fu, and Yi Yang. Soft filter pruning for accelerating deep convolutional neural networks. *arXiv preprint arXiv:1808.06866*, 2018. 2

[26] Peter Hedman, Pratul P Srinivasan, Ben Mildenhall, Jonathan T Barron, and Paul Debevec. Baking neural radiance fields for real-time view synthesis. In *Proceedings of the IEEE/CVF International Conference on Computer Vision*, pages 5875–5884, 2021. 2

[27] Byeongho Heo, Minsik Lee, Sangdoo Yun, and Jin Young Choi. Knowledge transfer via distillation of activation boundaries formed by hidden neurons. In *Proceedings of the AAAI Conference on Artificial Intelligence*, pages 3779–3787, 2019. 3

[28] Geoffrey Hinton, Oriol Vinyals, and Jeff Dean. Distilling the knowledge in a neural network. *arXiv preprint arXiv:1503.02531*, 2015. 3

[29] Tao Hu, Shu Liu, Yilun Chen, Tiancheng Shen, and Jiaya Jia. EfficientNeRF Efficient Neural Radiance Fields. In *Proceedings of the IEEE/CVF Conference on Computer Vision and Pattern Recognition*, pages 12902–12911, 2022. 2

[30] Bernhard Kerbl, Georgios Kopanas, Thomas Leimkühler, and George Drettakis. 3d gaussian splatting for real-time radiance field rendering. *ACM Transactions on Graphics (ToG)*, 42(4):1–14, 2023. 2, 3, 4, 6, 7, A9, A12, A13

[31] Arno Knapitsch, Jaesik Park, Qian-Yi Zhou, and Vladlen Koltun. Tanks and temples: Benchmarking large-scale scene reconstruction. *ACM Transactions on Graphics (ToG)*, 36 (4):1–13, 2017. 6, A9

[32] Sosuke Kobayashi, Eiichi Matsumoto, and Vincent Sitzmann. Decomposing nerf for editing via feature field distillation. *Advances in Neural Information Processing Systems*, 35:23311–23330, 2022. 3

[33] Georgios Kopanas, Julien Philip, Thomas Leimkühler, and George Drettakis. Point-based neural rendering with per-view optimization. In *Computer Graphics Forum*, pages 29–43. Wiley Online Library, 2021. 2, 3

[34] Yann LeCun, John Denker, and Sara Solla. Optimal brain damage. *Advances in neural information processing systems*, 2, 1989. 2

[35] Namhoon Lee, Thalaiyasingam Ajanthan, and Philip HS Torr. Snip: Single-shot network pruning based on connection sensitivity. *arXiv preprint arXiv:1810.02340*, 2018. 4

[36] Lingzhi Li, Zhen Shen, Zhongshu Wang, Li Shen, and Liefeng Bo. Compressing volumetric radiance fields to 1 mb. In *Proceedings of the IEEE/CVF Conference on Computer Vision and Pattern Recognition*, pages 4222–4231, 2023. 2, 5, 6, 7, A9, A10, A12, A13

[37] Lingjie Liu, Jiatao Gu, Kyaw Zaw Lin, Tat-Seng Chua, and Christian Theobalt. Neural Sparse Voxel Fields. *Advances in Neural Information Processing Systems*, 33:15651–15663, 2020. 2

[38] Yufan Liu, Jiajiong Cao, Bing Li, Chunfeng Yuan, Weiming Hu, Yangxi Li, and Yunqiang Duan. Knowledge distillation via instance relationship graph. In *Proceedings of the IEEE/CVF Conference on Computer Vision and Pattern Recognition*, pages 7096–7104, 2019. 3

[39] Chengzhi Mao, Lu Jiang, Mostafa Dehghani, Carl Vondrick, Rahul Sukthankar, and Irfan Essa. Discrete representations strengthen vision transformer robustness. *arXiv preprint arXiv:2111.10493*, 2021. 2

[40] Ben Mildenhall, Pratul P Srinivasan, Matthew Tancik, Jonathan T Barron, Ravi Ramamoorthi, and Ren Ng. Nerf: Representing Scenes As Neural Radiance Fields for View Synthesis. *Communications of the ACM*, 65(1):99–106, 2021. 1, 2, A9

[41] MPEGGroup. MPEG Point Cloud Compression - TMC13. https://github.com/MPEGGroup/mpeg-pcc-tmc13, 2022. 5

[42] Thomas Müller, Alex Evans, Christoph Schied, and Alexander Keller. Instant Neural Graphics Primitives With a Multiresolution Hash Encoding. *ACM Transactions on Graphics (TOG)*, 41:1 – 15, 2022. 2, 6, 7

[43] Ben Poole, Ajay Jain, Jonathan T Barron, and Ben Mildenhall. Dreamfusion: Text-to-3d using 2d diffusion. *arXiv preprint arXiv:2209.14988*, 2022. 3

[44] Christian Reiser, Songyou Peng, Yiyi Liao, and Andreas Geiger. Kilonerf: Speeding up neural radiance fields with thousands of tiny mlps. In *Proceedings of the IEEE/CVF International Conference on Computer Vision*, pages 14335–14345, 2021. 2, 3

[45] Adriana Romero, Nicolas Ballas, Samira Ebrahimi Kahou, Antoine Chassang, Carlo Gatta, and Yoshua Bengio. Fitnets: Hints for thin deep nets. *arXiv preprint arXiv:1412.6550*, 2014. 3

[46] Victor Sanh, Lysandre Debut, Julien Chaumond, and Thomas Wolf. Distilbert, a distilled version of bert: smaller, faster, cheaper and lighter. *arXiv preprint arXiv:1910.01108*, 2019. 3

[47] Katja Schwarz, Axel Sauer, Michael Niemeyer, Yiyi Liao, and Andreas Geiger. Voxgraf: Fast 3d-Aware Image Synthesis With Sparse Voxel Grids. *ArXiv Preprint ArXiv:2206.07695*, 2022. 2

[48] Sebastian Schwarz, Marius Preda, Vittorio Baroncini, Madhukar Budagavi, Pablo Cesar, Philip A Chou, Robert A Cohen, Maja Krivokuća, Sébastien Lasserre, Zhu Li, et al. Emerging mpeg standards for point cloud compression. *IEEE Journal on Emerging and Selected Topics in Circuits and Systems*, 9(1):133–148, 2018. 5

[49] Zhiqiang Shen, Zechun Liu, Dejia Xu, Zitian Chen, Kwang-Ting Cheng, and Marios Savvides. Is label smoothing truly incompatible with knowledge distillation: An empirical study. *arXiv preprint arXiv:2104.00676*, 2021. 3

[50] Vincent Sitzmann, Semon Rezchikov, William T. Freeman, Joshua B. Tenenbaum, and Frédo Durand. Light Field Networks: Neural Scene Representations With Single-Evaluation Rendering. *Advances in Neural Information Processing Systems*, 34, 2021. 2

[51] Cheng Sun, Min Sun, and Hwann-Tzong Chen. Direct Voxel Grid Optimization: Super-Fast Convergence for Radiance Fields Reconstruction. In *Proceedings of the IEEE/CVF Conference on Computer Vision and Pattern Recognition*, pages 5459–5469, 2022. 2, 6, A10

[52] Towaki Takikawa, Alex Evans, Jonathan Tremblay, Thomas Müller, Morgan McGuire, Alec Jacobson, and Sanja Fidler. Variable bitrate neural fields. In *ACM SIGGRAPH 2022 Conference Proceedings*, pages 1–9, 2022. 5

[53] Yonglong Tian, Dilip Krishnan, and Phillip Isola. Contrastive representation distillation. *arXiv preprint arXiv:1910.10699*, 2019. 3

[54] Aaron Van Den Oord, Oriol Vinyals, et al. Neural discrete representation learning. *Advances in neural information processing systems*, 30, 2017. 2

[55] Huan Wang, Yijun Li, Yuehai Wang, Haoji Hu, and Ming-Hsuan Yang. Collaborative distillation for ultra-resolution universal style transfer. In *Proceedings of the IEEE/CVF conference on computer vision and pattern recognition*, pages 1860–1869, 2020. 3

[56] Huan Wang, Jian Ren, Zeng Huang, Kyle Olszewski, Menglei Chai, Yun Fu, and Sergey Tulyakov. R2l: Distilling neural radiance field to neural light field for efficient novel view synthesis. In *European Conference on Computer Vision*, pages 612–629. Springer, 2022. 2, 3

[57] Jianqiang Wang, Dandan Ding, Zhu Li, and Zhan Ma. Multiscale point cloud geometry compression. In *2021 Data Compression Conference (DCC)*, pages 73–82. IEEE, 2021. 5

[58] Lin Wang and Kuk-Jin Yoon. Knowledge distillation and student-teacher learning for visual intelligence: A review and new outlooks. *IEEE transactions on pattern analysis and machine intelligence*, 44(6):3048–3068, 2021. 3

[59] Liao Wang, Jiakai Zhang, Xinhang Liu, Fuqiang Zhao, Yanshun Zhang, Yingliang Zhang, Minye Wu, Jingyi Yu, and Lan Xu. Fourier PlenOctrees for Dynamic Radiance Field Rendering in Real-Time. In *Proceedings of the IEEE/CVF Conference on Computer Vision and Pattern Recognition*, pages 13524–13534, 2022. 2

[60] Zirui Wu, Tianyu Liu, Liyi Luo, Zhide Zhong, Jianteng Chen, Hongmin Xiao, Chao Hou, Haozhe Lou, Yuantao Chen, Runyi Yang, et al. Mars: An instance-aware, modular and realistic simulator for autonomous driving. *arXiv preprint arXiv:2307.15058*, 2023. 1

[61] Dejia Xu, Yifan Jiang, Peihao Wang, Zhiwen Fan, Yi Wang, and Zhangyang Wang. Neurallift-360: Lifting an in-the-wild 2d photo to a 3d object with 360 {\deg} views. *arXiv preprint arXiv:2211.16431*, 2022. 3

[62] Wang Yifan, Felice Serena, Shihao Wu, Cengiz Öztireli, and Olga Sorkine-Hornung. Differentiable surface splatting for point-based geometry processing. *ACM Transactions on Graphics (TOG)*, 38(6):1–14, 2019. 3

[63] Alex Yu, Ruilong Li, Matthew Tancik, Hao Li, Ren Ng, and Angjoo Kanazawa. Plenoctrees for real-time rendering of neural radiance fields. In *Proceedings of the IEEE/CVF International Conference on Computer Vision*, pages 5752–5761, 2021. 2, 5

[64] Alex Yu, Sara Fridovich-Keil, Matthew Tancik, Qinhong Chen, Benjamin Recht, and Angjoo Kanazawa. Plenoxels: Radiance Fields Without Neural Networks. *2022 IEEE/CVF Conference on Computer Vision and Pattern Recognition (CVPR)*, pages 5491–5500, 2022. 2, 6, 7

[65] Sergey Zagoruyko and Nikos Komodakis. Paying more attention to attention: Improving the performance of convolutional neural networks via attention transfer. *arXiv preprint arXiv:1612.03928*, 2016. 3

[66] Richard Zhang, Phillip Isola, Alexei A Efros, Eli Shechtman, and Oliver Wang. The unreasonable effectiveness of deep features as a perceptual metric. In *Proceedings of the IEEE conference on computer vision and pattern recognition*, pages 586–595, 2018. 6

[67] Tianli Zhao, Jiayuan Chen, Cong Leng, and Jian Cheng. Tinynerf: Towards 100 x compression of voxel radiance fields. In *Proceedings of the AAAI Conference on Artificial Intelligence*, pages 3588–3596, 2023. 5

[68] Tinghui Zhou, Richard Tucker, John Flynn, Graham Fyffe, and Noah Snavely. Stereo magnification: Learning view synthesis using multiplane images. *arXiv preprint arXiv:1805.09817*, 2018. 1